Design of a Model Predictive Controller for formation flight on quasi-Halo orbits

Francesco Paolo Salzo — Ph.D. Candidate, Università di Pisa, Department of Information Engineering, 56122, Pisa, Italy. francesco.salzo@phd.unipi.it

Giordana Bucchioni — Assistant Professor, Università di Pisa, Department of Information Engineering, 56122, Pisa, Italy. giordana.bucchioni@unipi.it

Rafael Vazquez — Professor, Universidad de Sevilla, Department of Aerospace Engineering, 41092, Seville, Spain. rvazquez1@us.es

ABSTRACT

This paper presents a Model Predictive Control (MPC) approach for satellite formation flying around Halo orbits, exploiting the dynamics of the quasi-halo orbits in the context of the Circular Restricted Three-Body Problem (CR3BP), utilizing a relative dynamics model based on the Local Vertical Local Horizontal (LVLH) coordinate frame. The dynamics of quasi-halo orbits are analyzed, proposing an MPC solution, optimized for real-time satellite autonomy and dynamic space environments. The MPC controller demonstrated its effectiveness in trajectory recovery tasks, with its performance sensitivity to cost function weights revealing crucial trade-offs between maneuver time and fuel consumption.

Keywords: CR3BP; Quasi-Halo; NRHO; MPC; Formation flight

Nomenclature

$\mathcal{S}$	=	Synodic frame
$\mathcal{L}$	=	Local Vertical Local Horizontal (LVLH) frame
M_1, M_2	=	primary masses
μ	=	primaries mass ratio
$\boldsymbol{\rho}$	=	relative position vector
$\boldsymbol{r}_L$	=	position of the leader satellite
$\boldsymbol{r}_C$	=	position of the chaser satellite
$\boldsymbol{r}_h$	=	position of the targeted orbit
$\boldsymbol{\omega}_{l/i}$	=	angular velocity of the LVLH frame
$\boldsymbol{u}(t)$	=	control vector
$\boldsymbol{x}(t)$	=	spacecraft state
$\boldsymbol{A}(\boldsymbol{x})$	=	State transition matrix
$\boldsymbol{B}(\boldsymbol{x})$	=	Input matrix

1 Introduction

Formation flight among multiple satellites in orbit has become a cornerstone of modern space technology development. The concept of a distributed satellite system, comprising several smaller satellites, is lauded for its superior performance and enhanced reliability. Such configurations are designed to withstand the loss of individual agents without compromising the mission's overall success. The applications of these systems are diverse, spanning scientific research, Earth observation [1], and the burgeoning field of telecommunications satellite constellations [2].

On the other hand, the cislunar space — the region encompassing Earth and the Moon — is witnessing a rapid expansion in the use of distributed systems, underpinning the future of space exploration and utilization. The Lunar Gateway, a critical element of NASA's Artemis program, exemplifies this expansion. Scheduled to occupy a Near Rectilinear Halo Orbit (NRHO) around the Earth-Moon L_2 point, the Gateway offers a prime case study for this investigation. NRHOs are highly elongated orbits within the Halo family, providing distinctive characteristics and stability for formation flight. The quasi-halo orbits, quasi-periodic trajectories in the proximity of halo orbits, present an attractive proposition for formation flight due to their inherent stability and fuel efficiency. These orbits have been extensively studied in the field of astrodynamics, with the computation of quasi-periodic tori being achieved through the GMOS algorithm [3].

Fuel-centric rendezvous and formation flying strategies near libration points have been researched in the past. [4] describes the preliminary design of a phasing trajectory in a cislunar environment. The use of invariant manifold connections has been explored [5], and surrogate models have been developed to streamline global optimization efforts [6]. Comparisons between classical phasing and manifold connections for fuel efficiency have also been conducted [7]. In contrast, safety-focused close-rendezvous operations are increasingly gaining attention in the literature. [8] introduced a targeting law merged with a navigation filter. [9] suggested practical rendezvous scenarios for Earth-Moon Halo orbits. Shooting methods targeting rendezvous are explored in [10]. Notably, most of these studies employ the Earth-Moon co-rotating frame, which isn't optimal for describing target-specific state constraints. This shortfall justifies the broader use of local frames in close rendezvous, as noted in [11]. In this context, [12] proposed a Moon-centric local frame, considering the Lunar Gateway's practical Moon orbit. [13] proposed a safe automatic rendezvous strategy using this reference frame. Recently, the feasibility and controller design for chemically propelled satellite formation flight in cislunar space was studied in [14].

Model Predictive Control (MPC) leverages a system model to predict future behavior over a receding horizon and optimize control sequences based on a cost function [15]. MPC ensures effective handling of constraints and, if well-designed, has a feasible computational load, thus being ideal for real-time satellite autonomy in dynamic space environments. In recent years it has been extensively studied for various spacecraft control scenarios, including attitude control and station keeping [16], rendezvous maneuvers [17], and formation flight [18].

The work presented in this paper considers spacecraft equipped with electric propulsion, employing relative dynamics models in the Local Vertical Local Horizontal (LVLH) frame. The dynamics of quasi-halo orbits are analyzed, proposing a MPC solution, optimized for real-time satellite autonomy and dynamic space environments, leveraging the Circular Restricted Three-Body Problem (CR3BP) as our foundational dynamical model. The paper presents some initial findings with a basic MPC design, that will serve as the initial step to more robust designs, as remarked upon in Section 6.

The paper is structured as follows. Section 2 presents the CR3BP model, orbit computation methods, and the controller's basics for managing formation flight. Next, Section 3 deals with the study of quasi-halo orbits, their dynamics, practical applications, and controller design. Section 5 then presents the simulation results of our controller's performance. We finish in Section 6 with some concluding remarks and future ideas.
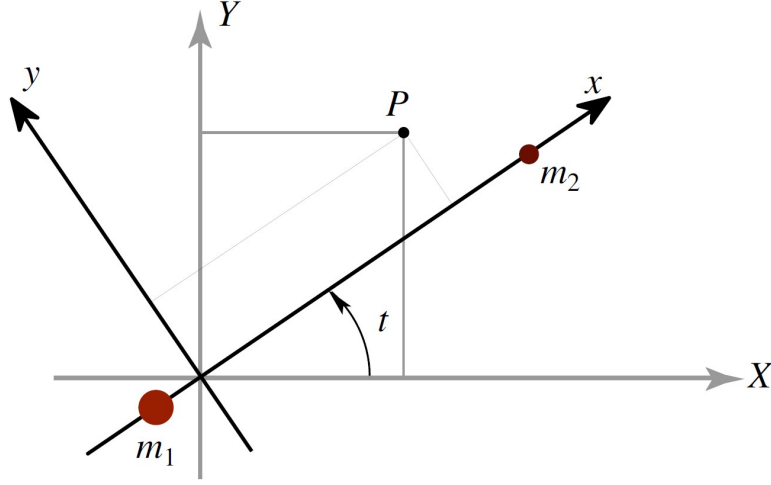
Fig. 1 Inertial and rotating frames (adapted from [19])

2 Dynamic Model

In this section, the model of the three-body problem in its simplified circular restricted form is initially presented. Following this, the periodic and quasi-periodic orbits of interest within this model are introduced. Lastly, the section discusses the relative motion problem between two satellites, presenting both the nonlinear and linearized equations for this scenario.

2.1 The CR3BP model

The Circular Restricted Three-Body Problem (CR3BP) is a simplification of the dynamics of the problem in which the two primaries, Earth and the Moon, revolve around their center of mass in circular orbits and are the only two sources of gravitational influence considered. The system is defined by the gravitational parameters of the two primaries μ_1 and μ_2 respectively and consequently by the primaries mass ratio μ. Consider an inertial frame, denoted as $I = \{O; \hat{\imath}_I, \hat{\jmath}_I, \hat{k}_I\}$, centered on the center of mass of the primary bodies, where the plane formed by the unit vectors $\hat{\imath}_I$ and $\hat{\jmath}_I$, respectively for X and Y axes, coincides with the orbital plane, and $\hat{k}_I$ aligns with the system's rotational axis (Z-axis). Then, let's define a right-handed rotating synodic reference frame $S = \{O; \hat{\imath}_s, \hat{\jmath}_s, \hat{k}_s\}$ with the x-axis unit vector $\hat{\imath}_s$ points along the imaginary line connecting the two primaries, and directed towards the second one, the z-axis unit vector $\hat{k}_s$ coinciding with $\hat{k}_I$, and the y-axis unit vector $\hat{\jmath}_s$ completing the triad, as shown in Fig. 1. The equations of motion can be conveniently expressed in the synodic coordinates (x, y, z) and their time-derivatives, using the augmented potential defined as:

$$\bar{U}(x, y) = -\frac{1}{2}\left(\mu_1 r_1^2 + \mu_2 r_2^2\right) - \frac{\mu_1}{r_1} - \frac{\mu_2}{r_2} \tag{1}$$

with r_1 and r_2 distances of a point mass m from M_1 and M_2, resulting in the following system:

$$\begin{cases} \ddot{x} - 2\dot{y} = -\bar{U}_x \\ \ddot{y} + 2\dot{x} = -\bar{U}_y \\ \ddot{z} = -\bar{U}_z \end{cases} \tag{2}$$

where $\bar{U}_x, \bar{U}_y, \bar{U}_z$ denote the partial derivatives of $\bar{U}$ with respect to x, y, z respectively.
The CR3BP admits five points of equilibrium, the Lagrangian points, three of them (L_1, L_2 and L_3) lie on the x-axis of the rotating frame and are called collinear points while L_4 and L_5 are the equilateral
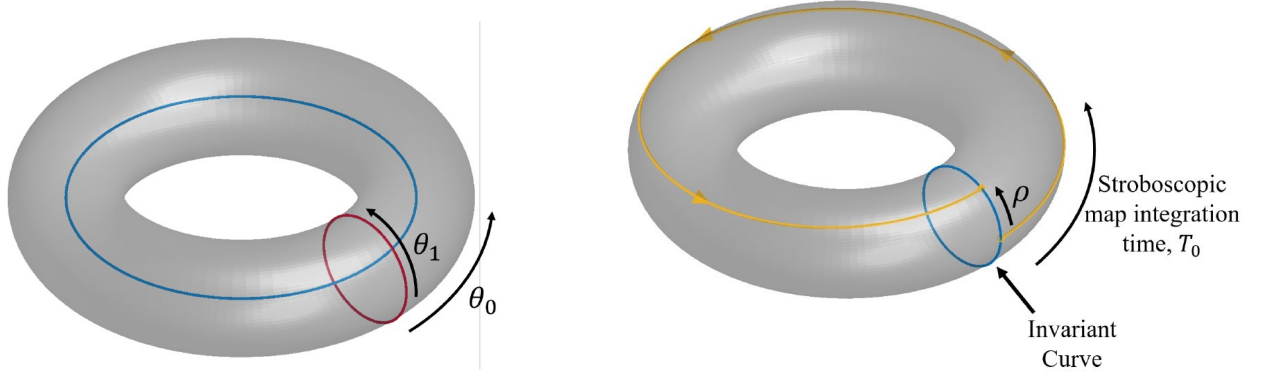
Fig. 2 **2-dimensional torus with latitudinal (red) and longitudinal (blue) invariant curves on the left, propagated trajectory (yellow) on the right (adapted from [20])**

points. Of particular significance among these are the collinear points L1 and L2, as they give rise to various families of periodic orbits. One notable family within these is the Halo orbits, which can be further categorized into southern and northern Halo families. Within the Halo orbit families, the Near Rectilinear Halo Orbits (NRHO) stand out due to their remarkable elongation and intriguing stability properties. In both practical applications and scientific studies, the 9:2 lunar synodic resonant NRHO within the Southern L2 Halo family, which closely approaches the lunar north pole with a periselene radius of ~ 3225 km and a period of about 6.5 days, is the preferred choice. This orbit has also been selected for the Lunar Gateway project.

2.2 Quasi-periodic orbits

Let's introduce the concept of quasi-periodic orbits associated with 2-dimensional invariant tori. From an eigenvalue perspective, these orbits are characterized by two complex conjugate eigenvalues with unit norm, indicating a center-center-saddle dynamics. Unlike periodic orbits, which reside on 1-dimensional tori with a single fundamental frequency (the inverse of the revolution period), quasi-periodic orbits on 2-dimensional tori feature two fundamental frequencies: the longitudinal frequency $\dot{\theta}_0$, and the latitudinal frequency $\dot{\theta}_1$.

Using a stroboscopic map, a quasi-periodic orbit trajectory can be represented as a curve on this torus as shown in Fig. 2, starting from the first latitudinal curve and progressing along the longitudinal direction across the entire torus. Given the mapping time T_0 and the angle of rotation ρ, the state vector $\boldsymbol{u}$ undergoes a rotation of ρ, satisfying:

$$\boldsymbol{u}(0, \theta_0, \theta_1) = \boldsymbol{u}(T_0, \theta_0, \rho + \theta_1) \tag{3}$$

The periodic orbit traces a trajectory in $\mathbb{R}^6$ space around the reference periodic orbit. A rotation operator $\boldsymbol{R}$ can be defined as:

$$\boldsymbol{R}(-\rho)\boldsymbol{u}(T_0, \theta_0, \theta_1) - \boldsymbol{u}(0, \theta_0, \theta_1) = 0 \tag{4}$$

The GMOS algorithm, as described in [20], is utilized to compute quasi-Halo orbits. An initial guess is generated using the Multiple-Shooting correction scheme. This scheme discretizes two invariant curves into patches: the longitudinal curve with M equally spaced points in time and the latitudinal curve with N states. This yields multiple quasi-Halo orbits that adhere to continuity constraints. Another constraint is required to specify the desired family. Specifically, we calculated families of quasi-halo orbits with a constant mapping time. The initial guess is obtained via the Monodromy Matrix at the perimoon of the reference periodic Halo orbit. The correction process follows, involving the Jacobian matrix, and the

pseudo-arc-length continuation scheme is subsequently used to find the next family initial guess.

2.3 Relative motion equations

In the context of this study, at a generic instant, two satellites are considered: a leader L in a NRHO orbit, and a chaser C, for which it is desired to be in point H along a quasi-halo orbit. Let r_L, r_C, and r_h represent their respective positions relative to the synodic frame. The relative motion is described using the Local Vertical Local Horizontal (LVLH) frame, as presented in [12]. The LVLH frame provides a more intuitive and physically meaningful way to analyze the relative motion of the vehicles.

It is convenient to define the LVLH frame centered in the targeted orbit position H as $\mathcal{L} = \{r_h; \hat{\imath}, \hat{\jmath}, \hat{k}\}$
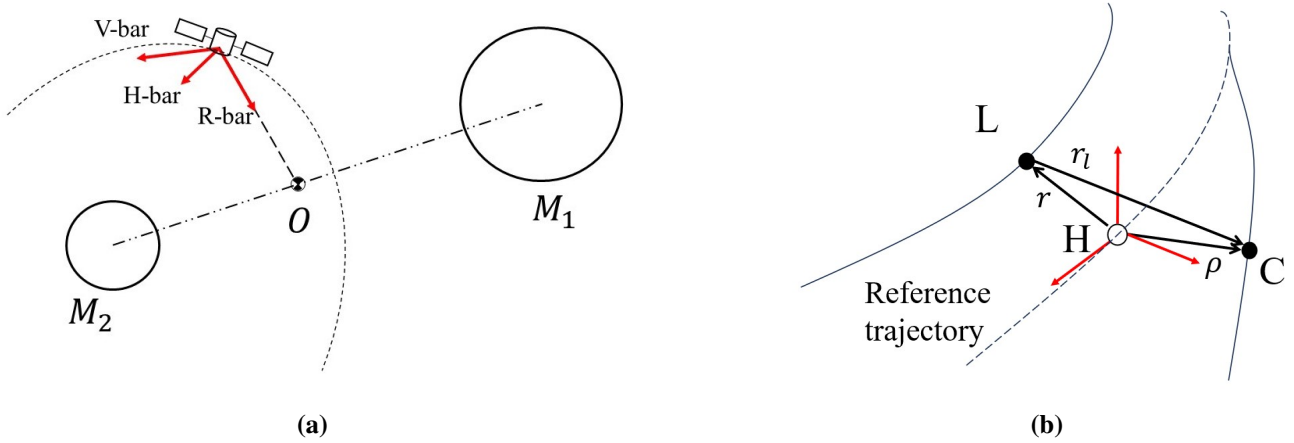

Fig. 3 (a) LVLH frame configuration with respect to the synodic frame and (b) with respect to the positions of leader and chaser.

defined based on the synodic reference frame, then $\hat{k}$ (R-bar) is pointing towards the center of mass O, $\hat{\jmath}$ (H-bar) points in the opposite direction of the angular momentum of the corresponding point at the origin of the LVLH reference frame and as a result $\hat{\imath}$ (V-bar). Starting from the relative position of the chaser satellite from the origin of the LVLH frame ρ, it is possible to obtain the following equation:

$$
\begin{aligned}
[\ddot{\rho}]_{\mathcal{I}} = & -2\omega_{l/i} \times [\dot{\rho}]_{\mathcal{I}} - \omega_{l/i} \times (\omega_{l/i} \times \rho) - \dot{\omega}_{l/i} \times \rho \\
& + (1 - \mu) \left(\frac{r_h - R_1}{\|r_h - R_1\|^3} - \frac{r_h + \rho - R_1}{\|r_h + \rho - R_1\|^3} \right) \\
& + \mu \left(\frac{r_h - R_2}{\|r_h - R_2\|^3} - \frac{r_h + \rho - R_2}{\|r_h + \rho - R_2\|^3} \right)
\end{aligned}
\tag{5}
$$

where R_1 and R_2 are the positions of the two primaries in the synodic frame and whose norms are $R_1 = \mu$ and $R_2 = 1 - \mu$, $\omega_{l/i}$ is the angular velocity of the local LVLH frame with respect to the inertial one and $[\dot{\omega}_{l/i}]_{\mathcal{L}}$ its derivative in $\mathcal{L}$.

These quantities can be expressed as a function of r_h and $\dot{r}_h$ with respect to the synodic frame (see [12]). The equation is nonlinear in ρ due to the term associated with gravitational acceleration, so we will refer to this set of equations as Nonlinear Equations of Relative Motion (NERM). To streamline controller design and improve computational efficiency, given that operations are conducted in the vicinity of the reference orbit that is $|\rho| \ll |r_h|$, the dynamics are linearized around the reference system's origin,

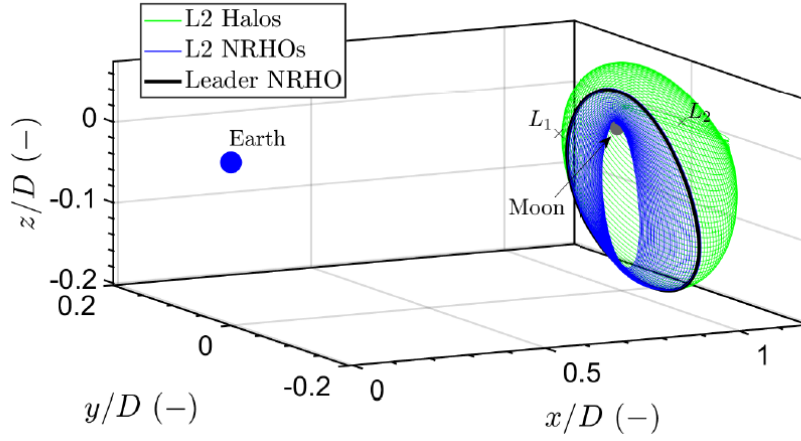**Fig. 4   Illustration of the NRHO in the Earth-Moon system (adapted from [21])**

resulting in the Linear Equations of Relative Motion (LERM):

$$[\ddot{\boldsymbol{\rho}}]_{\mathcal{I}} = -2\boldsymbol{\omega}_{l/i} \times [\dot{\boldsymbol{\rho}}]_{\mathcal{I}} - \boldsymbol{\omega}_{l/i} \times (\boldsymbol{\omega}_{l/i} \times \boldsymbol{\rho}) - \dot{\boldsymbol{\omega}}_{l/i} \times \boldsymbol{\rho}$$
$$- \left(\frac{1-\mu}{\|\boldsymbol{r}_h - \boldsymbol{R_1}\|^3} \bar{\boldsymbol{H}}_1 + \frac{\mu}{\|\boldsymbol{r}_h - \boldsymbol{R_2}\|^3} \bar{\boldsymbol{H}}_2 \right) \boldsymbol{\rho} \tag{6}$$

where:

$$\bar{\boldsymbol{H}}_i = \boldsymbol{I}_{3\times3} - 3\frac{(\boldsymbol{r_h} - \boldsymbol{R_i}) \otimes (\boldsymbol{r_h} - \boldsymbol{R_i})}{\|\boldsymbol{r_h} - \boldsymbol{R_i}\|^2} \tag{7}$$

with $i = 1, 2$. Let's define $\boldsymbol{u}(t) \in \mathbb{R}^3$ the control vector and $\boldsymbol{x}(t) \in \mathbb{R}^6$ the spacecraft state as $\boldsymbol{x} = \left[\boldsymbol{\rho}^T, \dot{\boldsymbol{\rho}}^T \right]^T$. Then the relative dynamics can be expressed in matrix form as a linear time-varying system:

$$\dot{\boldsymbol{x}}(t) = \begin{bmatrix} \boldsymbol{0}_{3\times3} & \boldsymbol{I}_{3\times3} \\ \boldsymbol{A}_{\rho}(t) & -2\boldsymbol{\Omega}_{l/i}(t) \end{bmatrix} \boldsymbol{x}(t) + \begin{bmatrix} \boldsymbol{0}_{3\times3} \\ \boldsymbol{I}_{3\times3} \end{bmatrix} \boldsymbol{u}(t) \tag{8}$$

where $\boldsymbol{\Omega}_{l/i}$ is the skew matrix of angular velocity $\boldsymbol{\omega}_{l/i}$ and $\dot{\boldsymbol{\Omega}}_{l/i}$ represents its derivative:

$$\boldsymbol{A}_{\rho} = -\boldsymbol{\Omega}_{l/i}^2 - \left[\dot{\boldsymbol{\Omega}}_{l/i} \right]_{\mathcal{L}} - \frac{1-\mu}{\|\boldsymbol{r_h} - \boldsymbol{R_1}\|^3} \bar{\boldsymbol{H}}_1 - \frac{\mu}{\|\boldsymbol{r_h} - \boldsymbol{R_2}\|^3} \bar{\boldsymbol{H}}_2 \tag{9}$$

3 Quasi-Halo orbits computation and selection

The choice of an appropriate reference orbit plays a critical role in the design and implementation of formation flight missions. In the following sections, we will delve into the details of selecting and characterizing the quasi periodic torus associated with the NRHO as our reference orbit, considering mission objectives, and assessing its compatibility with autonomous formation flight. The 9:2 synodic resonant L2 southern NRHO was calculated using the built-in function of the SEMpy Python library [22], with an initial periselene radius of 3225.11 km. The resulting orbit has a period $T = 157.50$ h, a Jacobi Constant $J = 3.05865$, and initial state in synodic coordinates given by $\boldsymbol{r}_0 = [3.9281e5, 0, -6.9958e4]^T$ km and $\boldsymbol{v}_0 = [0, -0.1053, 0]^T$ km/s. The pair of complex conjugate eigenvalues associated with the calculated orbit is $\lambda_{c_{1,2}} = 0.6845 \pm 0.7290$.

In order to compute the quasi periodic tori the GMOS differential correction algorithm was implemented in Python. Due to the high eccentricity of these orbits, the dynamics near the periselene is very fast and
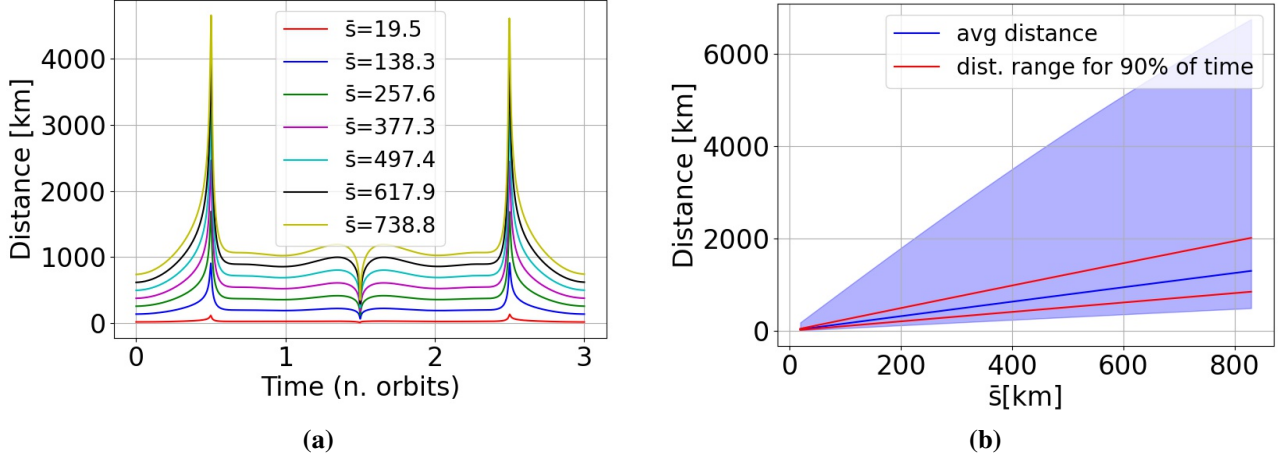
Fig. 5 **Distances from the central NRHO orbit of a sample of computed quasi-halos propagated from the aposelene over three NRHO periods (a), and distances from the central NRHO, displaying the average, maximum, and minimum distances as a function of $\bar{s}$ (b).**

leads to computational issues for the differential correction scheme. For this reason, despite calculating the monodromy matrix at the periselene after one orbit, the origin of the longitudinal curve is located at the aposelene of the NRHO orbit and thus it corresponds to the angle $\theta_0 = 0°$. In the initialization

Initialization				Continuation
M	N	ϵ	ρ_0	δ_s
5	26	1×10^{-3}	0.8168 rad/orbit	2×10^{-3}

Table 1 **Parameter Settings for Initialization and Continuation**

and continuation of the two-dimensional torus, the parameters detailed in Tab. 1 were employed. A total of 55 tori were computed with increasing aposelene distances. For each torus, we computed 26 quasi-halo orbits, which we will refer to either by numbering from 1 to 26 or by specifying the angle values of θ_1 for $\theta_0 = 0$. Each torus is uniquely labeled based on the distance $\bar{s}$ of the point corresponding to $\theta_0 = 0$ and $\theta_1 = 0$ from the NRHO orbit. The distance between the quasi-halos and the central NRHO orbit over the period is influenced by the dynamics, which exhibit rapid changes near periselene. At this point, the distances increase significantly, as seen in Fig. 5a. However, this effect is short-lived. As assessed in [23] and illustrated in Fig. 5b, as the parameter $\bar{s}$ increases, the maximum distance also increases rapidly. Still, it's essential to note that, for 90% of the period, the motion remains confined within a much narrower range. This behavior can be attributed to the dynamics near the periselene, as indicated in the figures. The torus with $\bar{s} = 302.4$ km was chosen for the purpose of this study. A more comprehensive analysis was conducted to explore the dynamics of the computed quasi-halo orbits, aiming to identify motion patterns and evaluate the potential for executing a multi-satellite formation flight on the quasi-periodic torus. An initial observation focused on the symmetry of the quasi-halo orbit No. 1 (0°/0°) over three orbital periods, as depicted in Fig. 6. It was noted that the trajectory exhibited symmetry with respect to the $x = 0$ plane of the LVLH reference frame and that with quasi halo No. 14 (0°/180°) exhibited a diametrically opposite and symmetric trajectory, with the angle between them remaining close to 180°for most of the time as showed in Fig. 7. These characteristics support their selection for forming a stable and equidistant three-satellite formation with the leader in the center and two chasers diametrically opposite.

In a broader context, the 26 quasi-halo orbits are explored for potential configurations accommodating more satellites on non collinear arrangements with specific angles (β) or fixed average distances (d).
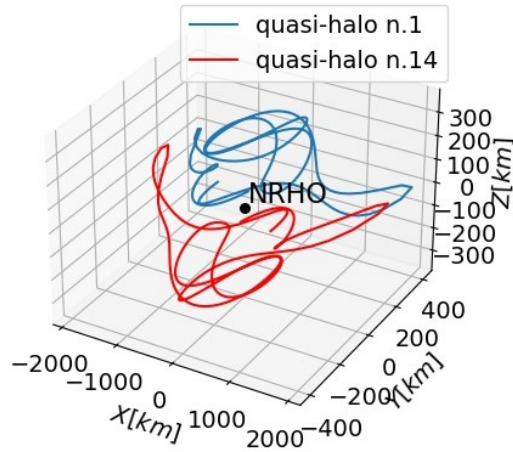
Fig. 6   Trajectories of quasi-halo orbits No. 1 (0°/0°) and No. 14 (0°/180°) over three orbital periods.
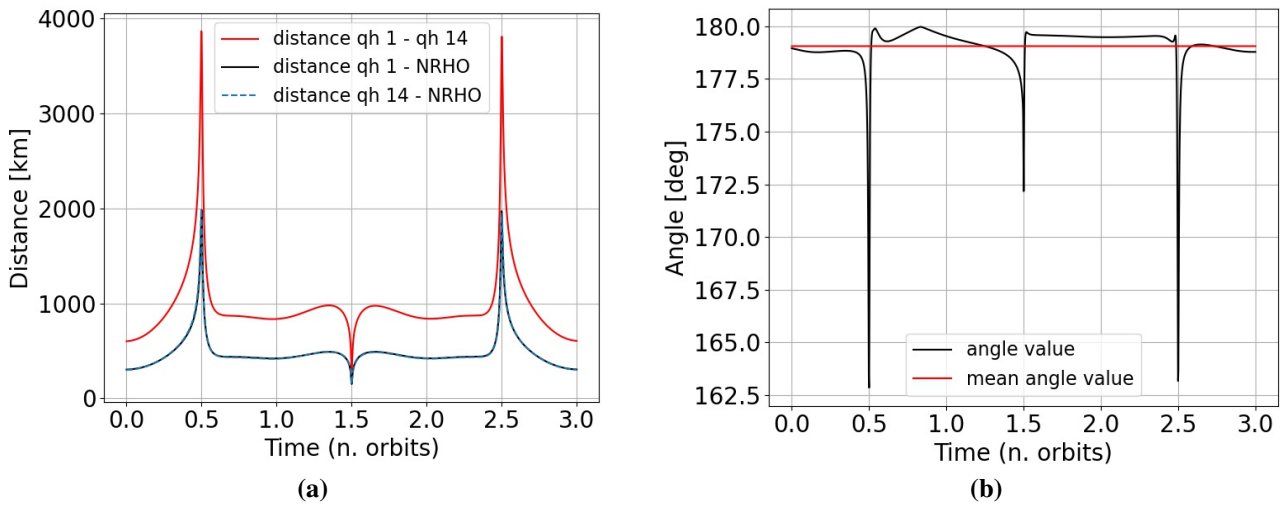

(a)

(b)

Fig. 7   (a) Distances of a sample of computed quasi-halos propagated from the aposelene over three NRHO periods, and (b) distances from the central NRHO, displaying the average, maximum, and minimum distances as a function of $\bar{s}$.
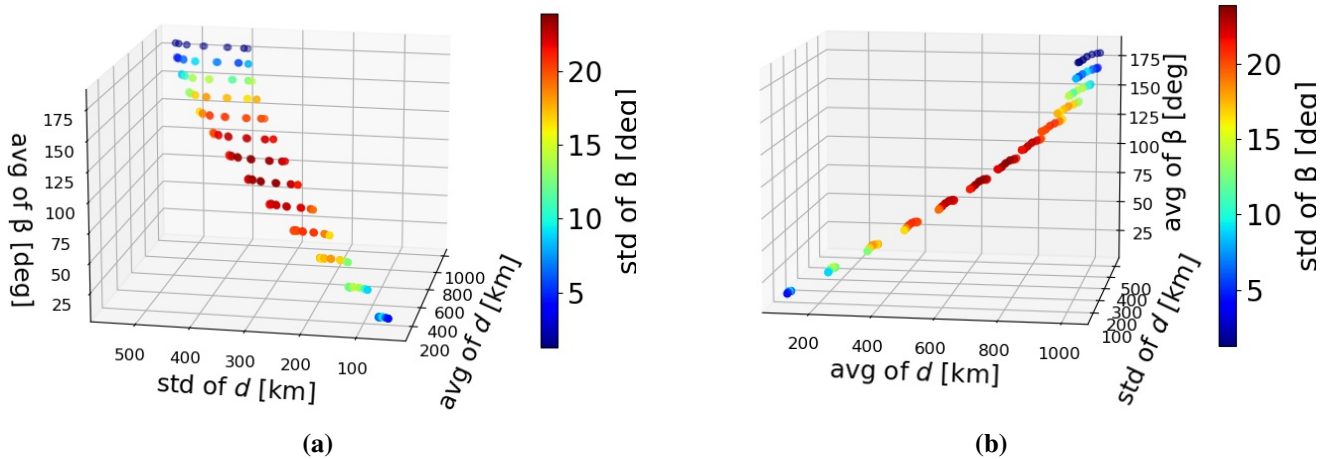

(a)

(b)

Fig. 8   Scatter plot showing the relationship between relative distance variability, angle variability, and mean angle for each pair of quasi-halo orbits

8

Analyzing the orbits in pairs, we assess their performance over a three-period duration, focusing on key metrics such as the average and standard deviation of relative distances and angles. The results of these analyses are visualized through a scatter plot in Fig. 8, where the x and y axes represent the mean and standard deviation of distances, and the z-axis displays the mean β angle. The color bar indicates the standard deviation of the angle. Notably, we observe that smaller angles ($< 30°$ and $> 150°$) exhibit low standard deviations, indicating stable, aligned formations. On the other hand, configurations with angles close to $90°$ display higher variability, challenging formation stability.

This analysis allows us to select orbit combinations that minimize inter-satellite distance and angle variability, thereby enhancing overall formation performance.

4 Model Predictive Control for formation flight

In the following section, the design of the MPC controller for a single chaser, in the configuration depicted in Fig. 3b, will be introduced. The designed controller's performance will then be assessed through simulations in the subsequent section.

4.1 Cost Function

The discrete nature of Model Predictive Control requires the discretization of the continuous system. In this context, we employed Radau collocation on finite elements, which is a direct, simultaneous, and full discretization approach, to derive the equivalent discrete system with respect to time:

$$x_{k+1} = A(x_k)x_k + B(x_k)u_k \tag{10}$$

where k is the current time instant. We adopted a Receding Horizon approach, shifting the prediction horizon $[k, k + N_p]$ as the control process unfolds. In our research, we considered the case of electric propulsion, involving continuous and low-thrust maneuvers approximated by a sequence of discrete control inputs.

The control problem at each time step t_i is defined by the cost function (J) which includes terms for position error (ρ_k), control input (u_k), and control input variations (Δu_k). The cost function also minimizes propellant consumption and ensures stable tracking of the reference trajectory.

$$J = \sum_{k=i}^{i+N_p-1} \left(\rho_k^T \mathbb{W}_{l_\rho} \rho_k + u_k^T \mathbb{W}_{l_u} u_k + \Delta u_k^T \mathbb{R} \Delta u_k \right) + x_{i+N}^T \mathbb{W}_m x_{i+N} \tag{11}$$

where N_p is the prediction horizon. In the control design, we focus on minimizing position errors ($\rho_k^T \mathbb{W}_{l_\rho} \rho_k$) within the Lagrangian term. This emphasizes the precise tracking of desired trajectories to achieve formation flight objectives. In contrast, the stabilizing term V_f considers both position and velocity to ensure overall orbit stability ($x_{i+N}^T \mathbb{W}_m x_{i+N}$). The term $\Delta u_k^T \mathbb{R} \Delta u_k$ penalizes abrupt changes in acceleration, promoting smoother control actions, while the term $u_k^T \mathbb{W}_{l_u} u_k$ optimizes propellant consumption, critical for extended mission durations.

4.2 Constraints

A constraint on the maximum thrust the propulsion system can deliver is implemented. The constraint is anisotropic to maintain quadratic problem properties, however, it would overestimate the actual maximum possible input by a factor of $\sqrt{3}$, so, given the real maximum thrust limit in acceleration $\bar{U}$, for each component we set $u_{max} = \frac{\bar{U}}{\sqrt{3}}$. Then the constraint equation read as:

$$-u_{max} \leq u_i \leq u_{max}, \quad i = 1, 2, 3 \tag{12}$$

9

A nonlinear collision avoidance constraint has been introduced to enhance the overall safety of the formation flight, designating a zone around the main satellite that must be avoided to prevent potential collisions. The collision avoidance constraint was implemented using the following bound inequality:

$$-\|\boldsymbol{\rho} - \boldsymbol{r}\|_2 < -R_{co} \tag{13}$$

In the absence of a more sophisticated model, R_{co} should be chosen to be greater than the minimum distance reached between the satellites at perilune. Otherwise, the satellite will need to execute maneuvers that result in a larger distance error in the region immediately following perilune.

4.3 Mass estimation

Finally a simple method for determining the propellant mass m_{prop} is needed. Following the approach used in [24], assuming factors such as the initial spacecraft mass m_0 and the specific Impulse I_{sp}, and calculating the ΔV from the control velocities, the Tsiolkovsky equation can be used:

$$m_p = m_0 \left(1 - e^{-\frac{\Delta V}{I_{sp}g}}\right) \tag{14}$$

where we need to estimate the value of ΔV. Given the number of steps of the simulation N_{steps} and the time step t_{step}. it can be roughly computed as:

$$\Delta V = \Delta V_x + \Delta V_y + \Delta V_z \tag{15}$$

$$\Delta V_j = \sum_{k=1}^{N_{steps}} |u_j| t_{step} \tag{16}$$

where j represents the directions x, y, and z.

t_{step}	N	δr	δv	u_{max}	$\mathbb{W}_{l_\rho}$		$\mathbb{W}_{l_u}$		$\mathbb{W}_m$		$\mathbb{R}$
6 min	50	50 km	0 km/s	10^{-4} m/s^2	10^5	$\boldsymbol{I}_{3\times3}$	0.3	$\boldsymbol{I}_{3\times3}$	10^6	$\boldsymbol{I}_{6\times6}$	$\boldsymbol{I}_{6\times6}$

Table 2   Simulation parameters

5 Results

In the following section, we consider the case of a leader satellite in an NRHO orbit and a chaser with the quasi-halo (0°/0°) as the reference orbit. The LERM equation (Eq. 6) will be used for the MPC model, while the plant model will encompass the complete set of NERM equations (Eq. 5). To address the optimization problem, the open-source nonlinear optimization package Ipopt (Interior Point Optimizer), integrated into the do-mpc library [25] has been employed. For larger problems with numerous variables, the default MUMPS solver is a recommended choice, as evaluated by [26].

It is assumed that the leader satellite is capable of performing station-keeping in its NRHO orbit. The time step was selected as a compromise between mitigating discretization errors and accounting for the problem's dynamics. Parameters used for the following simulations are shown in Tab. 2. Finally, reasonable values were considered for the chaser satellite, such as $m_0 = 250$ kg and $I_{sp} = 3000$ s.

Simulations were conducted on a computer equipped with an Intel Core i7-8750H processor and revealed that solving each MPC optimization problem step takes between 230 ms and 450 ms. This computational time depends on the system's dynamics. Near the aposelene region, the optimizer converges faster, resulting in shorter computation times while requiring more time near the periselene region. Importantly,
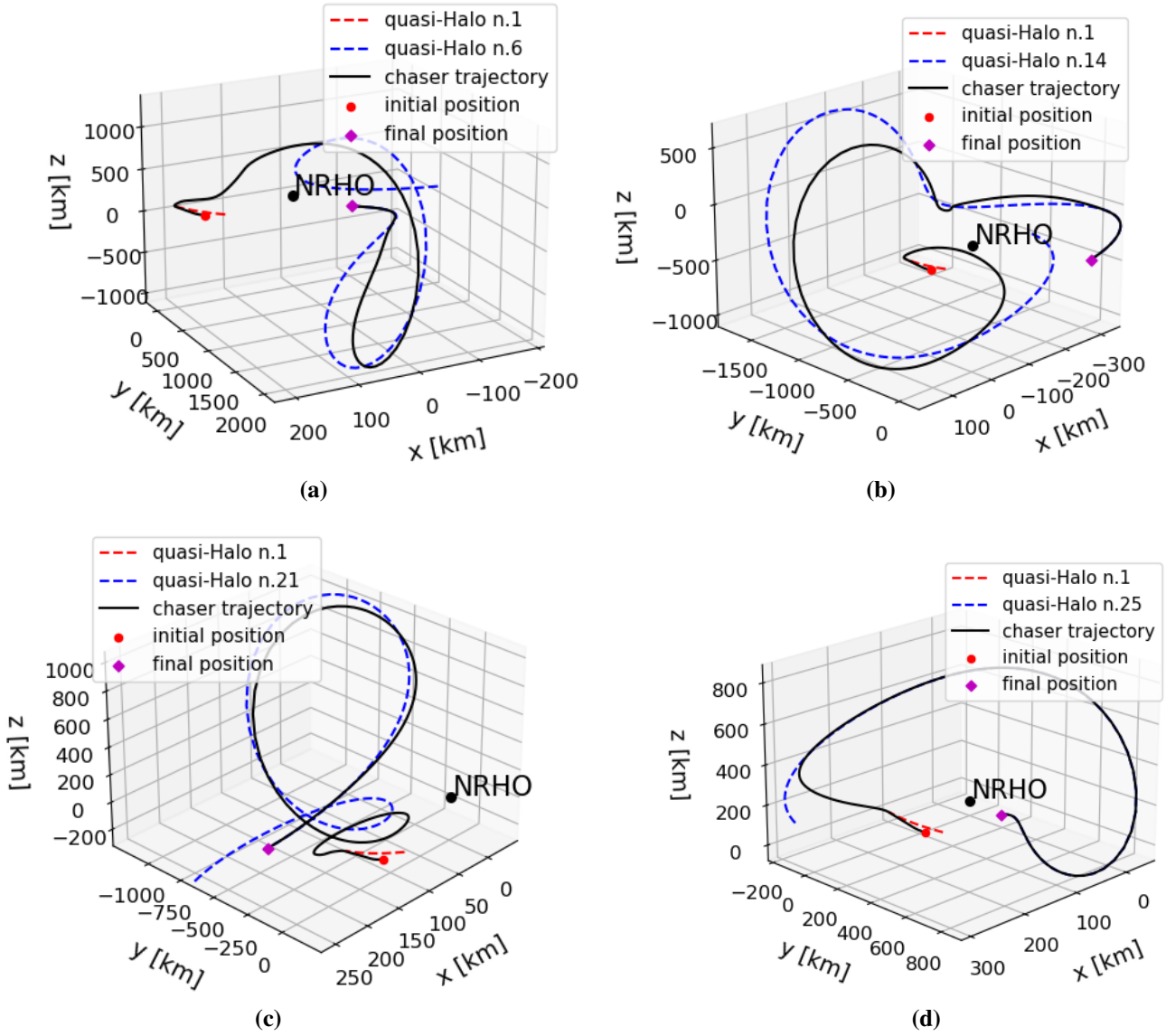
10

Fig. 9 **Transfer maneuvers from quasi-halo 1 to:** **(a) quasi-halo 6; (b) quasi-halo 14; (c) quasi-halo 21; (d) quasi-halo 25.**

the computational time remains significantly lower than the MPC controller's time step of 6 minutes for all simulated scenarios. The controller has been tested for two fundamental maneuvers: trajectory recovery in the presence of an initial disturbance and orbital transfer to another quasi-halo orbit.

5.1 Transfer Maneuvers

Regarding the transfer maneuver, the initial reference orbit is quasi-halo No. 1 (0°/0°), and the most challenging transfer is to quasi-halo No. 14 (0°/180°), diametrically opposite. A sample of transfer trajectories is shown in Fig. 9. All transfer maneuvers start shortly after the aposelene.

It was observed that while the controller can execute all transfers if initiated within approximately 20 hours after the aposelene, it encounters difficulties in transferring to the more distant orbits if the starting time is significantly delayed after the aposelene.
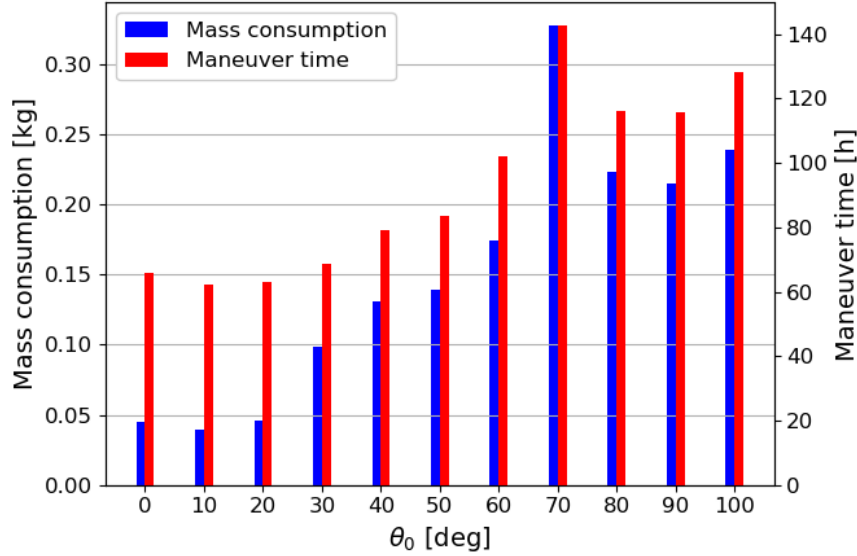
Fig. 10   Performance in recovery maneuver of the reference orbit

5.2 Reference orbit recovery

A Monte Carlo simulation was conducted to assess the chaser's ability to return to its reference orbit following an initial disturbance of 100 km in magnitude. The starting point along the orbit, represented by the angle θ_0, was systematically varied at intervals of 10°. For each θ_0 angle, five simulations were carried out, with the direction of the perturbation vector randomly selected from the entire 4π solid angle. Due to the intensive computational demands, the number of simulations could not be further increased. The time required for the maneuver and the propellant consumption were measured as performance indicators, and the results are shown in Fig. 10. To optimize computation time, the focus was placed on analyzing the controller's performance using only the portion of the orbit that spanned from aposelene to periselene. This approach leveraged the fact that if the controller succeeded in this part of the orbit, it was likely to function effectively in the second part, from periselene to aposelene. Moreover, conducting simulations starting very close to the periselene with the same disturbance was infeasible, as even a small initial disturbance in this region could lead to significant changes in the motion dynamics.

5.3 Weight sensitivity in controller performance

The analysis examined various weight combinations to determine how changes in Lagrangian weights affected the controller's ability to optimize flight time and fuel consumption. The results are illustrated in Fig. 11. The chosen weight intervals were kept close to the values in Tab. 2, as significant deviations during the initial tuning phase resulted in controller instability and ineffective maneuver. The graphs confirm the significance of this choice, showing an exponential relationship between propellant consumption and the weight associated with control input, as well as between maneuver time and the weight associated with position. A slight decrease in the positional weight, can result in a substantial increase in flight time, eventually leading to controller instability and an inability to complete the maneuver. On the other hand, the dependence on the weight of the control input appears to exhibit a linear behavior.
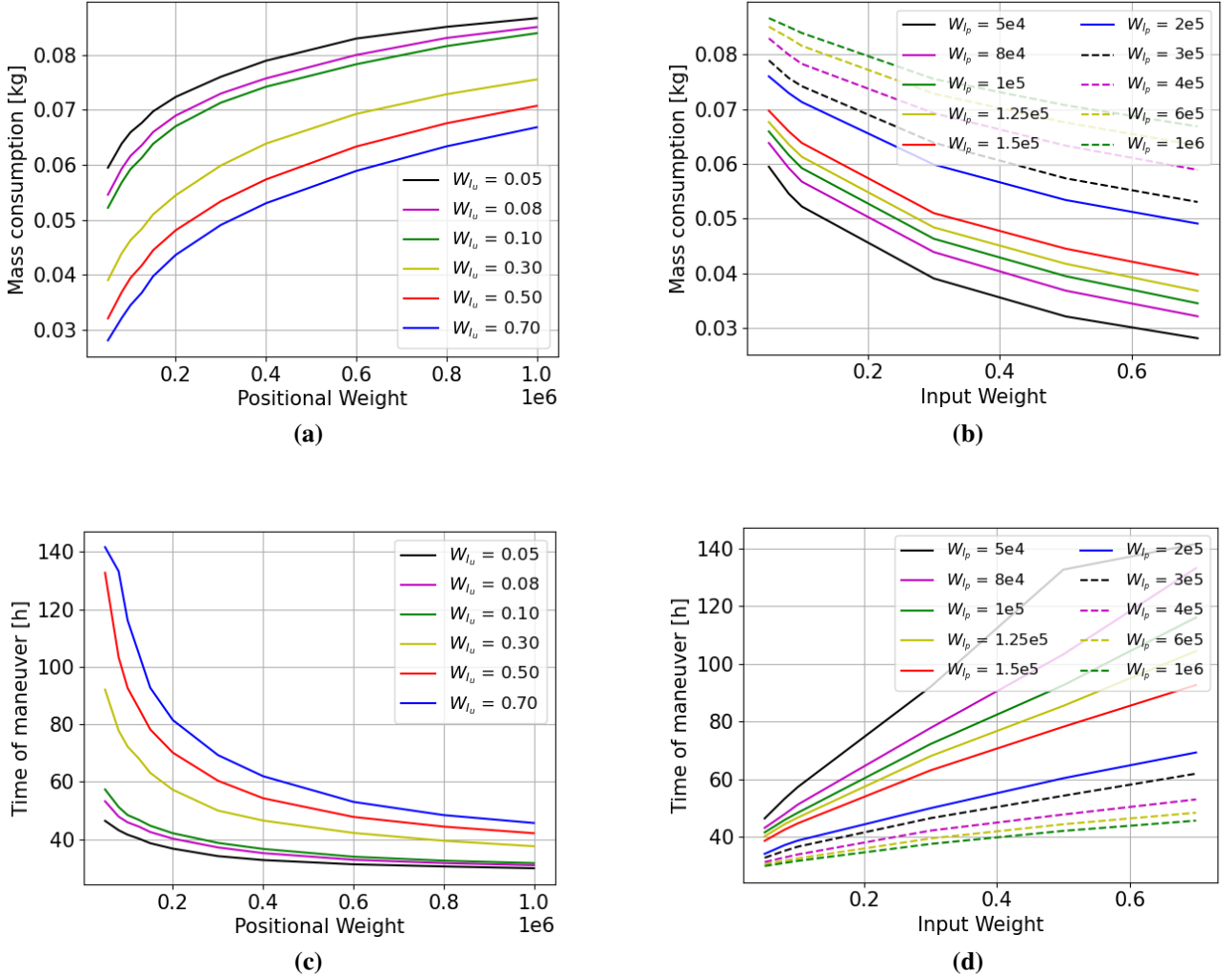
12

Fig. 11 Relationship between Lagrangian weights and controller performance

6 Conclusion and Future works

This study investigated the viability of low-thrust propulsion in conjunction with a Model Predictive Control (MPC) approach for satellite formation flying in the context of the CR3BP. By examining the dynamics of quasi-halo orbits, the research identified stable configurations for formations of single or even multiple satellites. The MPC controller demonstrated its effectiveness in trajectory recovery tasks, with its performance sensitivity to cost function weights revealing crucial trade-offs between maneuver time and fuel usage. While the computational burden of the MPC is demonstrably lower than the simulation time step, it remains an aspect requiring optimization for onboard execution on resource-limited satellite platforms. Future endeavors will focus on validating this control strategy against high-fidelity models and refining state estimation through integrated estimators. In addition, we aim to extend the scope of our current study by advancing the design of a robust rendezvous controller specifically tailored for the complexities of the CR3BP environments. Drawing inspiration from established robust control strategies in Keplerian rendezvous, such as the chance-constrained method and Halo orbit management techniques [21, 27–29], we plan to adapt the robust method delineated in [30] for R3BP. Our approach will integrate a stochastic parameter estimator with a Model Predictive Control (MPC) framework [31], facilitating real-time recalibrations that respond to disturbances, thereby enhancing control precision. Furthermore, an exploration of chaser propulsion types—whether chemical or electrical—will be incorporated into our research.

Acknowledgments

References

[1] Marco D'Errico. *Distributed space missions for earth system monitoring*, volume 31. Springer Science & Business Media, 2012. DOI: 10.1007/978-1-4614-4541-8.

[2] Saptarshi Bandyopadhyay, Rebecca Foust, Giri P Subramanian, Soon-Jo Chung, and Fred Y Hadaegh. Review of formation flying and constellation missions using nanosatellites. *Journal of Spacecraft and Rockets*, 53(3):567–578, 2016. DOI: 10.2514/1.A33291.

[3] Zubin P Olikara and Daniel J Scheeres. Numerical method for computing quasi-periodic orbits and their stability in the restricted three-body problem. *Advances in the Astronautical Sciences*, 145(911-930):911–930, 2012.

[4] Giordana Bucchioni and Mario Innocenti. Phasing maneuver analysis from a low lunar orbit to a near rectilinear halo orbit. *Aerospace*, 8(3):70, 2021. DOI: 10.3390/aerospace8030070.

[5] G. Gomez, W. S. Koon, M. W. Lo, J. E. Marsden, J. Masdemont, and S. D. Ross. Connecting orbits and invariant manifolds in the spatial restricted three-body problem. *Nonlinearity*, 17(5):1571–1606, 2004. DOI: 10.1088/0951-7715/17/5/002.

[6] Haijun Peng, Chunfeng Yang, Yunpeng Li, Sheng Zhang, and Biaosong Cheng. Surrogate-based parameter optimization and optimal control for optimal trajectory of Halo orbit rendezvous. *Aerospace Science and Technology*, 26(1):176–184, 2013. DOI: 10.1016/j.ast.2012.04.001.

[7] Yuki Sato, Kenji Kitamura, and Takeya Shima. Spacecraft Rendezvous Utilizing Invariant Manifolds for a Halo Orbit. *Transactions of the Japan Society for Aeronautical and Space Sciences*, 58(5):261–269, 2015. DOI: 10.2322/tjsass.58.261.

[8] Brian L. Jones and Robert H. Bishop. Rendezvous Targeting and Navigation for a Translunar Halo Orbit. *Journal of Guidance, Control and Dynamics*, 17(5):1109–1114, 1994. DOI: 10.2514/3.21317.

[9] Naomi Murakami, Satoshi Ueda, Toshinori Ikenaga, Maki Maeda, Toru Yamamoto, and Hitoshi Ikeda. Practical rendezvous scenario for transportation missions to cis-lunar station in Earth-Moon L2 Halo orbit. In *25th International Symposium on Space Flight Dynamics (ISSFD)*, Munich, Germany, 2015.

[10] Stephanie Lizy-Destrez, Laurent Beauregard, Emmanuel Blazquez, Antonino Campolo, Sara Manglativi, and Victor Quet. Rendezvous Strategies in the Vicinity of Earth-Moon Lagrangian Points. *Frontiers in Astronomy and Space Sciences*, 5(45):1–19, 2019. DOI: 10.3389/fspas.2018.00045.

[11] Wigbert Fehse. *Automated Rendezvous and Docking of Spacecraft*, pages 171–215. Cambridge University Press. Cambridge, UK, 1 edition, 2003. DOI: 10.1017/CBO9780511543388.

[12] Giovanni Franzini and Mario Innocenti. Relative motion dynamics in the restricted three-body problem. *Journal of Spacecraft and Rockets*, 56(5):1322–1337, 2019. DOI: 10.2514/1.A34390.

[13] Giordana Bucchioni and Mario Innocenti. Rendezvous in cis-lunar space near rectilinear halo orbit: Dynamics and control issues. *Aerospace*, 8(3):68, 2021. DOI: 10.3390/aerospace8030068.

[14] Andrea Capannolo, Giovanni Zanotti, Michèle Lavagna, and Giuseppe Cataldo. Model predictive control for formation reconfiguration exploiting quasi-periodic tori in the cislunar environment. *Nonlinear Dynamics*, 111(8):6941–6959, 2023. DOI: 10.1007/s11071-022-08214-8.

[15] David Q. Mayne James B. Rawlings and Moritz M. Diehl. *Model predictive control: theory, computation, and design*, volume 2.

[16] Ryan J Caverly, Stefano Di Cairano, and Avishai Weiss. Electric satellite station keeping, attitude control, and momentum management by mpc. *IEEE Transactions on Control Systems Technology*, 29(4):1475–1489, 2020.

[17] Edward N Hartley. A tutorial on model predictive control for spacecraft rendezvous. In *2015 European Control Conference (ECC)*, pages 1355–1361. IEEE, 2015.

[18] Julian Scharnagl, Panayiotis Kremmydas, and Klaus Schilling. Model predictive control for continuous low thrust satellite formation flying. *IFAC-PapersOnLine*, 51(12):12–17, 2018.

[19] Wang Sang Koon, Martin W. Lo, Jerrold E. Marsden, and Shane D. Ross. *Dynamical Systems, the Three-Body Problem and Space Mission Design*, pages 1167–1181. DOI: 10.1142/9789812792617$_0$222.

[20] Brian P McCarthy. *Characterization of quasi-periodic orbits for applications in the sun-earth and earth-moon systems*. PhD thesis, Purdue University Graduate School, 2019.

[21] Julio C Sanchez, Francisco Gavilan, and Rafael Vazquez. Chance-constrained model predictive control for near rectilinear halo orbit spacecraft rendezvous. *Aerospace Science and Technology*, 100:105827, 2020. DOI: 10.1016/j.ast.2020.105827.

[22] E Blazquez, T Gateau, and S Lizy-Destrez. Sempy: a python open-source toolbox for non-keplerian astrodynamics. In *International Conference on Astrodynamics Tools and Techniques (ICATT)*, 2021.

[23] Andrea Capannolo. *Dynamics, guidance and control of reconfigurable spacecraft formations in multibody environments*. PhD thesis, Polytechnic of Milan, 2022.

[24] Nicholas Hamilton, David Folta, and Russell Carpenter. Formation flying satellite control around the l2 sun-earth libration point. In *AIAA/AAS Astrodynamics Specialist Conference and Exhibit*, page 4528, 2002. DOI: 10.2514/6.2002-4528.

[25] Felix Fiedler, Benjamin Karg, Lukas Lüken, Dean Brandner, Moritz Heinlein, Felix Brabender, and Sergio Lucia. do-mpc: Towards fair nonlinear and robust model predictive control. *Control Engineering Practice*, 140:105676, 2023. DOI: 10.1016/j.conengprac.2023.105676.

[26] Byron Tasseff, Carleton Coffrin, Andreas Wächter, and Carl Laird. Exploring benefits of linear solver parallelism on modern nonlinear optimization applications. *arXiv preprint arXiv:1909.08104*, 2019. DOI: 10.48550/arXiv.1909.08104.

[27] Francisco Gavilan, Rafael Vazquez, and Eduardo Fernandez Camacho. Chance-constrained model predictive control for spacecraft rendezvous with disturbance estimation. *Control Engineering Practice*, 60:111–122, 2012. DOI: 10.1016/j.conengprac.2011.09.006.

[28] Cristophe Louembet, Denis Arzelier, and Georgia Deaconu. Robust Rendezvous Planning Under Maneuver Execution Errors. *Journal of Guidance, Control and Dynamics*, 38(1):76–93, 2015. DOI: 10.2514/1.G000391.

[29] M. Mammarella, E. Capello, H. Park, C. Guglieri, and M. Romano. Tube-based robust model predictive control for spacecraft proximity operations in the presence of persistent disturbance. *Aerospace Science and Technology*, 77:585–594, 2018. DOI: 10.1016/j.ast.2018.04.009.

[30] Francisco Gavilan, Rafael Vazquez, and Eduardo F Camacho. Robust model predictive control for spacecraft rendezvous with online prediction of disturbance bounds. *Proceedings of AGNFCS'09*, 2011.

[31] Eduardo Fernandez Camacho and Carlos Bordons. *Model Predictive Control*, chapter 9, pages 249–287. Springer-Verlag, London, 2 edition, 2004. DOI: 10.1007/978-0-85729-398-5.

16